Supplementary Information

Lucas Casparis[1], Andreas Fuhrer[2], Dorothée Hug[1], Dominikus Kölbl[1], and Dominik M. Zumbühl[1]

[1]*Department of Physics, University of Basel, Klingelbergstrasse 82, CH-4056 Basel, Switzerland and*
[2]*IBM Research, Zürich Research Laboratory, Säumerstrasse 4, CH-8803 Rüschlikon, Switzerland*
(Dated: March 17, 2017)

In this supplementary section we present detailed information about the geometry of all samples and the transport measurements on these samples. Further we describe the method we applied for determining the current distribution in our samples. The results from these numerical calculations are then compared to the approximative method used in the main text.

I. GEOMETRY OF NANO GRAPHITE FLAKES

Table I and II summarize all sample geometries of the nanographite devices shown in Fig. 2 of the main text. For Madagascar Samples 4-9 no ρ_{ab} measurement was possible because no suitable contacts were available. Despite the missing separate ρ_{ab} measurement on those samples, we nevertheless correct for the in-plane contribution to R_c. We use $\rho_{ab} = 0.8\ \mu\Omega m$ as a fixed value and show values derived from this in parenthesis. Sample numbers 1 and 2 of every type of graphite are also included in Fig. 3 of the main text showing the temperature dependence. The solid (dashed) lines in this figure correspond to sample numbers 1 (2), respectively.

TABLE I: Nano-sample parameters for the determination of ρ_{ab}, see main text for definitions, and Fig. 1 therein for an illustration. Samples listed here are represented in Figs. 2 and 3. Fig. 3 shows the temperature dependence for samples 1 and 2 of each specimen.

Material	R_{ab} (Ω)	$A_{ab}(\mu m^2)$	$l_{ab}(\mu m)$	$\rho_{ab}(\mu\Omega m)$
HOPG 1	3.8	0.8	2.5	1.2
HOPG 2	5.6	0.45	3.3	0.8
India 1	18.9	0.25	7	0.7
India 2	67	0.8	10	5.3
Madagascar 1	7.6	1.5	8	1.5
Madagascar 2	11.8	0.3	6	0.6
Madagascar 3	9.1	0.8	8	0.9

TABLE II: Nano-sample parameters for the determination of ρ_c, see main text for definitions, and Fig. 1 therein for an illustration. Samples listed here are represented in Figs. 2 and 3. Fig. 3 shows temperature dependence for samples 1 and 2 of each specimen. For samples where no ρ_{ab} measurement was possible, values derived from a typical $\rho_{ab}=0.8\mu\Omega m$ are shown in parenthesis.

Material	$R_c(\Omega)$	$l_{cl}(\mu m)$	$w_l(\mu m)$	$l_{cu}(\mu m)$	$w_u(\mu m)$	$d(nm)$	$h(nm)$	$\widehat{R_c}(\Omega)$	$A_u(\mu m^2)$	$\rho_c(m\Omega m)$	R_A
HOPG 1	12	4	25	2.5	25	30	14	2.3	361	58	48k
HOPG 2	12	6	20	2	20	30	24	2.9	57	6.9	8.8k
India 1	19	1	20	3	20	15	17	11	100	63	89k
India 2	37	2.4	20	2	15	20	150	1.3	88	0.78	140
Madagascar 1	27	1.2	10	2.3	10	16	80	13	248	41	28k
Madagascar 2	26	4.2	8	3.3	5	14	37	5.6	95	15	24k
Madagascar 3	31	2.5	15	2	22	44	31	21	458	311	360k
Madagascar 4	68	6.5	26	2	20	10	26	(28)	200	(213)	(266k)
Madagascar 5	26	7	18	1	18	21	50	(11)	127	(28)	(35k)
Madagascar 6	100	2.6	16	2	12	20	330	(88)	92	(25)	(31k)
Madagascar 7	16	5.5	9	5.5	9	150	300	(8.5)	96	(2.7)	(3.4k)
Madagascar 8	9	4	15	6.2	8.5	100	450	(3.2)	140	(1)	(1.35k)
Madagascar 9	104	1	12	4.5	11	65	335	(101)	96	(28)	(35k)

II. NUMERICAL SIMULATION OF CURRENT DISTRIBUTION

The approximative method which is used to extract ρ_{ab}, ρ_c and ultimately R_A, includes several simplifications. In order to improve the extraction of these parameters, we numerically simulate the current flow for our sample geometries. The simulation allows us to determine ρ_{ab} taking into account the effectively reduced current carrying cross-section due to the point like contact geometries. Further, we can include the resistivity anisotropy in the simulation, enabling an estimate for the concentration of the current flow in the layers closest to the contacts, which again improves the determination of ρ_{ab}, ρ_c and R_A.

Combining Ohms law and the continuity equation gives:

$$0 = \dot{\rho} = \sigma \Delta \Phi \tag{1}$$

where we have assumed that sigma is a spatially constant tensor of the form:

$$\sigma = \begin{pmatrix} \sigma_{ab} & 0 & 0 \\ 0 & \sigma_{ab} & 0 \\ 0 & 0 & \sigma_c \end{pmatrix} \tag{2}$$

In order to solve equation (1) we map our samples to a rectangular, evenly spaced, grid. The typical grid spacing (da,db,dc) in the a- and b-direction is on the order of microns. For the c-direction a grid spacing of 0.5 nm is used. By rewriting the three dimensional grid as a vector, we reduce the calculation to the solution of a system of linear equations, which can be written in matrix form and subsequently solved using standard procedures i.e. Gaussian elimination.

The boundary conditions are chosen such that no current flows perpendicular to the sample boundary except at the contacts. This means $E_\perp = -\nabla \Phi_\perp = 0$ at the sample boundary where there are no contact pads. On the contact pads $E_\perp = -\nabla \Phi_\perp = $const and the bias current is evenly distributed over the contact-sample interface.

The fitting of the measured values is performed as follows: First, from the device and contact geometry of the R_{ab} measurement, the corresponding ρ_{ab}^{sim} is calculated as a function of the anisotropy ratio R_A. In a second step, taking into account the used contact geometry, the measured c-axis resistance R_c is simulated as a function of R_A. To calculate R_c, we assume the sample consists of two cuboids sitting on top of each other and split the calculation into two steps. The current is injected from a metal contact into the first cuboid and drained on the entire interface area of the two cuboids. For the second cuboid, the current is injected at the interface area and drained on a metal contact. We find that reducing the area where current flows from one cuboid into the other does not change our results by more than a few percent, validating the assumption of a homogenous current flow at the interface between the cuboids.

By matching the simulated $R_c(R_A)$ to the measured value R_c, we find R_A^{sim}. Together with the first calculation step this determines ρ_{ab}^{sim}. Knowing ρ_{ab}^{sim} and R_A^{sim}, we calculate ρ_c^{sim}.

Table III compares the results obtained through the approximative method with the ones extracted from the numerical calculation. For the samples where a R_{ab} measurement was not possible, we fixed $\rho_{ab}^{sim} = 50$ nΩm, in order to calculate ρ_c^{sim}. These values are again given in parenthesis. For two samples the numerical calculation did not converge, these values are omitted in Table III. The reason for the divergence in this two cases could be that ρ_{ab} is actually lower than the fixed ρ_{ab}^{sim}. By lowering the fixed ρ_{ab}^{sim} the simulation converges, but we omit these points, because R_A then highly depends on the fixed parameter.

As already stated in the main text the approximated ρ_{ab} presents an upper bound. This is confirmed by our simulation which give $\rho_{ab}^{sim} < \rho_{ab}$, ranging from ratios between ρ_{ab} and ρ_{ab}^{sim} of 6 (India 1) to 100 (India 2). We think the main reason for this deviation from the approximative method is the neglected anisotropy for the extraction of ρ_{ab}, which effectively reduces the current carrying cross-section A. This is confirmed by the observation that the reduction in ρ_{ab}^{sim} is largest, where R_{ab} is measured on the thickest samples (India 2, Madagascar 1), and smallest for the thinnest sample (India 1). Further, our rather point-like contact geometries have to be corrected for a spread in current, effectively changing the sample geometry in the ab-plane. This can be a relevant effect as we see in the calculated potential distribution in the ab-plane (not shown).

Because comparing the calculations and literature values, ρ_{ab}^{sim} is much smaller than previously measured in macroscopic samples [1–3]. Although in previous experiments more suitable contact geometries have been used to extract ρ_{ab}, we cannot exclude effects like the large anisotropy or current spread. This might explain the deviation between ρ_{ab}^{sim} and literature values.

Another reason for the low ρ_{ab}^{sim} in exfoliated, nanoscale samples could be the reduction of bulk disorder during exfoliation, actually suggested by our data and the disorder induced delocalization model. Further, an ab-measurement

TABLE III: Comparing approximated ρ_{ab}, ρ_c and R_A with numerically simulated values.

Material	ρ_{ab}(nΩm)	ρ_c(mΩm)	R_A	ρ_{ab}^{sim}(nΩm)	ρ_c^{sim}(mΩm)	R_A^{sim}
HOPG 1	1,200	58	48k	57	150	2,600k
HOPG 2	780	6.9	8.8k	48	37	780k
India 1	710	63	89k	120	84	680k
India 2	5,300	0.78	140	53	32	610k
Madagascar 1	1,500	41	28k	25	74	2,900k
Madagascar 2	600	15	24k	62	32	500k
Madagascar 3	860	310	360k	27	171	6,300k
Madagascar 4	(800)	210	(266k)	(50)		
Madagascar 5	(800)	28	(35k)	(50)	(85)	(1,700k)
Madagascar 6	(800)	25	(31k)	(50)		
Madagascar 7	(800)	2.7	(3.4k)	(50)	(4)	(80k)
Madagascar 8	(800)	1	(1.35k)	(50)	(0.8)	(16k)
Madagascar 9	(800)	28	(35k)	(50)	(39)	(780k)

in a macroscopic specimen will extend over several grain boundaries, whereas the multiply cleaved nanosamples are single or few grain graphite.

Despite some big deviations for ρ_{ab}, the simulations show that ρ_c^{sim} values are on the same order of magnitude as ρ_c, obtained using the approximative method. There seems to be a tendency of slightly higher ρ_c^{sim} (factor of 2-3), but this qualitative agreement clearly strengthens the approximative method to determine ρ_c. As an overall consequence, the numerically calculated R_A^{sim} is even higher than shown in the main text, reaching values up to 6,000,000 (Madagascar 3). Notably for India 2, for which we previously extracted a rather low $\rho_c \sim 0.8$ mΩm, now $\rho_c^{sim} \sim 53$ mΩm, in good agreement with all the other samples. Fig. 1 compares the two calculation methods graphically, including all samples measured. The results of the approximation already included in the main text, are plotted in weaker colours. The trend of the thickness dependence for numerically calculated (dashed line) and approximated ρ_c (dotted line) persists. The slopes of linear fits in the log-log plot lie within the corresponding error bars. The two data points for which the simulation did not converge were omitted in Figure 1.

[1] W. Primak and L. H. Fuchs, Phys. Rev. **95**, 22 (1954).
[2] L. Edman, B. Sundqvist, E. McRae, and E. Litvin-Staszewska, Phys. Rev. B**57**, 6227 (1998).
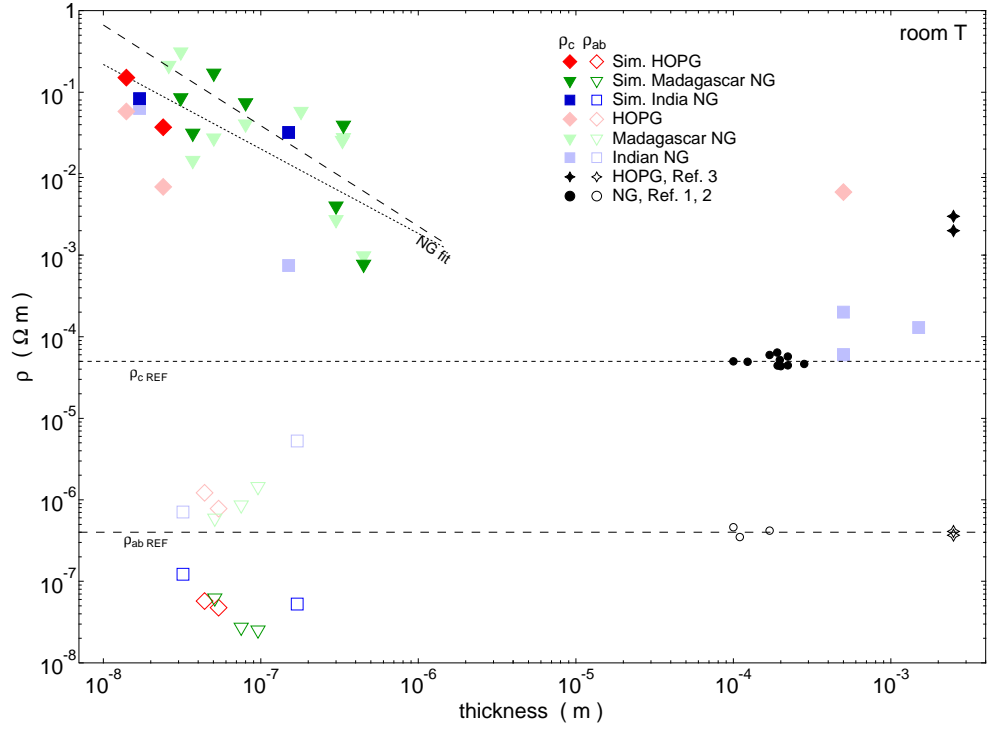[3] I. L. Spain, A. R. Ubbelohde, and D. A. Young, Phil. Trans. Royal Soc., Series A **345** (1967).

FIG. 1: Comparison of extraction method for ρ_c and ρ_{ab} at room temperature, comparing HOPG (red) with Madagascar NG (green) and Indian NG (blue). Filled, dark markers show ρ_c^{sim}, empty, dark markers display ρ_{ab}^{sim} both extracted using the anisotropic resistivity solver. Filled,light markers are ρ_c and empty, light makers indicated ρ_{ab}, evaluated using the estimate given and were already included in Fig 2 in the main text. For ρ_{ab} and ρ_{ab}^{sim}, the abscissa value is $d + h$, the overall flake thickness, see Table II. Previous measurements of macroscopic samples (black) were added for both HOPG [3] (stars) and NG [1, 2] (circles) for comparison. Dashed horizontal lines indicate literature values $\rho_{ab\,REF}$ for ρ_{ab} and $\rho_{c\,REF}$ for ρ_c. Further, the best power-law fits to all NG nanostep data (dotted line for ρ_c approximated in the main text, slope of -1.0 ± 0.4; dashed line for ρ_c^{sim} obtained with the simulation, slope of -1.2 ± 0.4;) are added to indicate a potential trend